



# Influences of superheat and cooling intensity on macrostructure and macrosegregation of duplex stainless steel studied by thermal simulation

Hong-gang Zhong<sup>1,2</sup> · Xiang-ru Chen<sup>1</sup> · Yan-jie Liu<sup>2</sup> · Zhi-qiang Wei<sup>1</sup> · Hai-feng Yu<sup>3</sup> · Qi-jie Zhai<sup>1,2</sup>

Received: 20 May 2020 / Revised: 27 July 2020 / Accepted: 9 August 2020 / Published online: 5 July 2021  
© China Iron and Steel Research Institute Group 2021

## Abstract

The influences of superheat and cooling intensity on macrostructure and macrosegregation of one new kind duplex stainless steel (DSS) were studied. Thermal simulation equipment was applied to prepare samples, which could reproduce the industrial processes of DSS manufactured by a vertical continuous slab caster. Macrostructure and macrosegregation were analyzed using the digital single lens reflex and laser-induced breakdown spectroscopy (LIBSOPA-200), respectively. The percentage of both chill zone and center equiaxed zone increases with the superheat decreasing, while that of the columnar zone decreases. There is only equiaxed grain existing as the superheat is 10 and 20 °C. The lower the superheat is, the coarser the grain size is. High cooling intensity in mold could remarkably decrease the chill zone length and refine the grains in chill zone and center equiaxed zone. The influences of cooling intensity on macrosegregation are greater than those of superheat. The macrosegregation of Si, Mn and Cr is slightly dependent on superheat, while that of Cu, Mo and Ni changes greatly with superheat increasing.

**Keywords** Continuous casting · Solidification · Thermal simulation · Duplex stainless steel · Macrosegregation

## 1 Introduction

Duplex stainless steel (DSS) with advantages of both austenitic and ferritic stainless steels [1] has been widely applied in ocean engineering, petroleum and chemical industries. DSS is going to replace austenitic or ferritic stainless steels due to the higher strength and better corrosion resistance [2, 3]. 2205 steel is one typical kind of DSS, containing 22 wt.% Cr and 5 wt.% Ni, which could take the place of 304 austenitic stainless steel in transportation pipelines and

chemical industry. Multiple lean DSS (2103 and 2002, etc.) has also been developed, which could be used in severe corrosive conditions, such as sea-crossing bridge [4].

Continuous casting (CC) is a low-cost and high-yield production mode compared with the mold casting and is often applied to produce DSS slabs. Typical solidification structures of CC slabs consist of three distinct zones: surface chill, inner columnar and central equiaxed crystal zones [5]. The macrostructure, especially high ratio of center equiaxed zone and fine grain size, is significant for the quality of CC slabs [5]. Many researches focus on the techniques of increasing equiaxed crystals [6–8]. It is reported that macrostructure is affected by casting parameters, such as superheat, cooling mode in mold and secondary cooling zone [9], electromagnetic stirring [10–12], pulse magneto-oscillation [13–17] and so on. Therefore, suitable continuous casting process is of great significance for high-quality billet production.

As for the new type DSS, it is necessary to propose suitable process parameters for industrial production. Commonly, the parameters are obtained from industrial tests or numerical simulation. The industrial tests, however,

✉ Hong-gang Zhong  
hgzhong@shu.edu.cn

✉ Xiang-ru Chen  
chenxr@shu.edu.cn

<sup>1</sup> Center for Advanced Solidification Technology, Shanghai University, Shanghai 200444, China

<sup>2</sup> Shanghai Institute of Materials Genome, Shanghai 200444, China

<sup>3</sup> Research Institute, Baoshan Iron & Steel Co., Ltd., Shanghai 200431, China

are costly and risky to damage the casting machine. For example, the leakage of steel or the breaking of billet due to the improper process causes huge maintenance costs more than the materials costs in the experiment and even leads to machine scrapping. And it is challengeable for the numerical simulation owing to the complicated non-equilibrium process of solidification. Zhong et al. [18, 19] have proposed a thermal simulation method to study the solidification process of continuous casting. One characteristic solidification unit is extracted as a thermal simulation sample based on the similarity of heat transformation during continuous casting. Solidification in mold is simulated by flip casting, and then the unsteady growth of dendrites is controlled by temperature gradient and growth rate of dendritic tip. The casting structure of the thermal simulation samples has been proved in good agreement with the actual continuous casting slabs [18]. And the parameters optimization by thermal simulation has been applied successively for ferritic stainless steel [19], high carbon steel [20], and even for the heat-resistant steel in mold casting [21].

In this study, the influence of superheat and cooling intensity on macrostructure and macrosegregation of a new type lean DSS was investigated by thermal simulation, which could make a contribution to industrial production.

## 2 Experimental

### 2.1 Experimental material

A new type lean DSS was experimented in this study, and the compositions are shown in Table 1. Different with the common 2205 DSS, the new DSS with lower mass percent of Cr and Ni possesses better plasticity and higher yield strength owing to the transformation-induced plasticity (TRIP) effect.

Some thermal physical parameters of DSS, calculated by JMatPro V8 software, are shown in Fig. 1, which is significant for numerical simulation, and would be applied to obtain the thermal field of CC slab. The liquidus and solidus temperatures were 1475 and 1390 °C, respectively, which could be reflected by the fraction of solid, as shown in Fig. 1a.

**Table 1** Compositions of new DSS (wt.%)

C	Si	Mn	Cr	Ni	Mo	Cu	N	Fe
0.027	0.37	1.38	20.34	2.95	1.13	0.33	0.07	Balance

### 2.2 Experimental parameters and procedure

In the study, all the experimental parameters were based on the industrial vertical continuous caster conditions, which are shown in Table 2. A thermal simulation (TS) equipment (as shown in Ref. [22]) designed by Zhai group was adopted. Previous researches have illustrated the principles and reasons to select TS samples [18]. The sample size, consequently, was 100 mm (half thickness of CC slab) × 15 mm × 5 mm.

As TS sample was put into the crucible, it was heated to 1550 °C and held for 20 min to ensure melting completely. Then, the temperature was kept at a target pouring temperature for 10 min. Later, the crucible was placed upside down to realize the in-suit pouring process. At that moment, molten metal encountered the water-cooled copper sidewall, and a chilled layer was rapidly formed. And sequentially TS sample was solidified with controlled cooling parameters in the high-temperature and low-temperature zones, respectively. The sample was stationary, while the heating unit moved away at a certain speed until solidification was complete during cooling process. The samples were taken from the furnace and cooled in the air when the samples were lower than 1200 °C. In the experiment, the sample was protected from oxidation by blowing argon.

Some previous studies have proved that TS samples could reflect the solidification characteristics of the industrial CC slabs by selecting the proper moving speed and cooling curves of heating unit [18, 19]. The moving speed was related to the growth speed of shell thickness of CC slab. And the cooling curves were controlled by the temperature distribution at the core of CC slab along with the casting direction. It was difficult to obtain the parameters directly owing to the high temperature and opacity. Consequently, numerical simulation was applied to calculate the relative parameters by ProCAST. The model was two-dimensional slice [23, 24].

To study the influences of superheat and cooling modes on the solidification process, five set parameters were used, respectively. The selected superheat was 10, 20, 30, 40 and 50 °C. Five set cooling modes are shown in Table 3, which were proposed based on the empirical water distribution model.

The cooling curves of the high-temperature zone and moving speed of heating unit calculated by numerical simulation are shown in Fig. 2. Figure 2a and c reveals the temperature variation and moving speed with the distance to meniscus at different superheats with cooling model III. Figure 2b and d shows the temperature and moving speed with different cooling models at 30 °C superheat. It has been demonstrated that the temperature of the low-temperature zone should be 110 °C lower than the liquidus

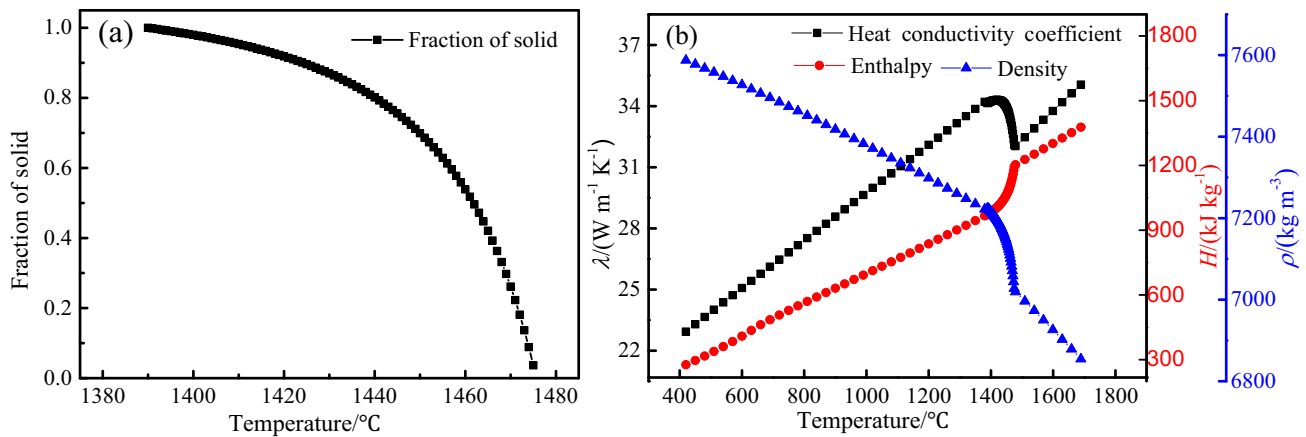


**Fig. 1** Thermal physical parameters calculated by JMatPro V8 software. **a** Fraction of solid; **b** heat conductivity coefficient ( $\lambda$ ), enthalpy ( $H$ ) and density ( $\rho$ )

temperature to ensure a reasonable temperature gradient [19]. The abscissa of Fig. 2, distance to meniscus ( $d$ ), could be transferred to time ( $t$ ) according to equation:

$$t = d/r, \quad (1)$$

where  $r$  is pulling rate of slab.

TS samples were sectioned in growth direction, then ground with diamond sandpaper and polished with 3.5- $\mu\text{m}$  abrasive paste. Canon-EOS 600D digital single lens reflex was applied to observe macrostructure after etching in the mixed solution of 15 g copper sulfate, 50 mL hydrochloric acid and 50 mL water for 90 s.

**Table 2** Main parameters of vertical continuous caster

Parameter	Value
Working mold length/m	0.8
Secondary cooling length/m	13.6
Section size of slab/(mm $\times$ mm)	200 $\times$ 1200
Pulling rate of slab/(m $\text{min}^{-1}$ )	0.8

**Table 3** Calculated heat conduction parameters of slab surface in each section

Cooling mode	Mold	Foot-roller section	Section of secondary cooling zone						
			1st	2nd	3rd	4th	5th	6th	7th
I (Strongest)	1400	965	670	460	340	270	220	135	90
II (Stronger)	1330	920	620	430	310	250	200	125	80
III (Industrial)	1220	835	570	390	280	220	170	105	70
IV (Weaker)	1110	750	520	350	250	190	140	95	70
V (Weakest)	1040	705	470	320	220	170	120	75	60

Macro-segregation was studied by the technique of in situ statistical analysis. The sectioned TS samples were inlaid in resin, polished with 400 grit abrasive paper and then scanned using a laser-induced breakdown spectroscopy (LIBSOPA-200) with a spot size of 300  $\mu\text{m}$  to analyze the area distribution of key elements.

## 3 Results and discussion

### 3.1 Macrostructure

The properties and qualities of the continuous cast slabs are related to macrostructure. In this research, the influences of two primary processing parameters, superheat and cooling intensity, on macrostructure are considered. As shown in Table 3, cooling mode III is close to the industrial condition. Consequently, when the superheat is studied, the cooling intensity is cooling mode III and stays in the same. As the cooling intensity changes, the superheat maintains at 30  $^{\circ}\text{C}$ . The macrostructure of DSS solidified with different superheat and cooling intensities is shown in Fig. 3. The

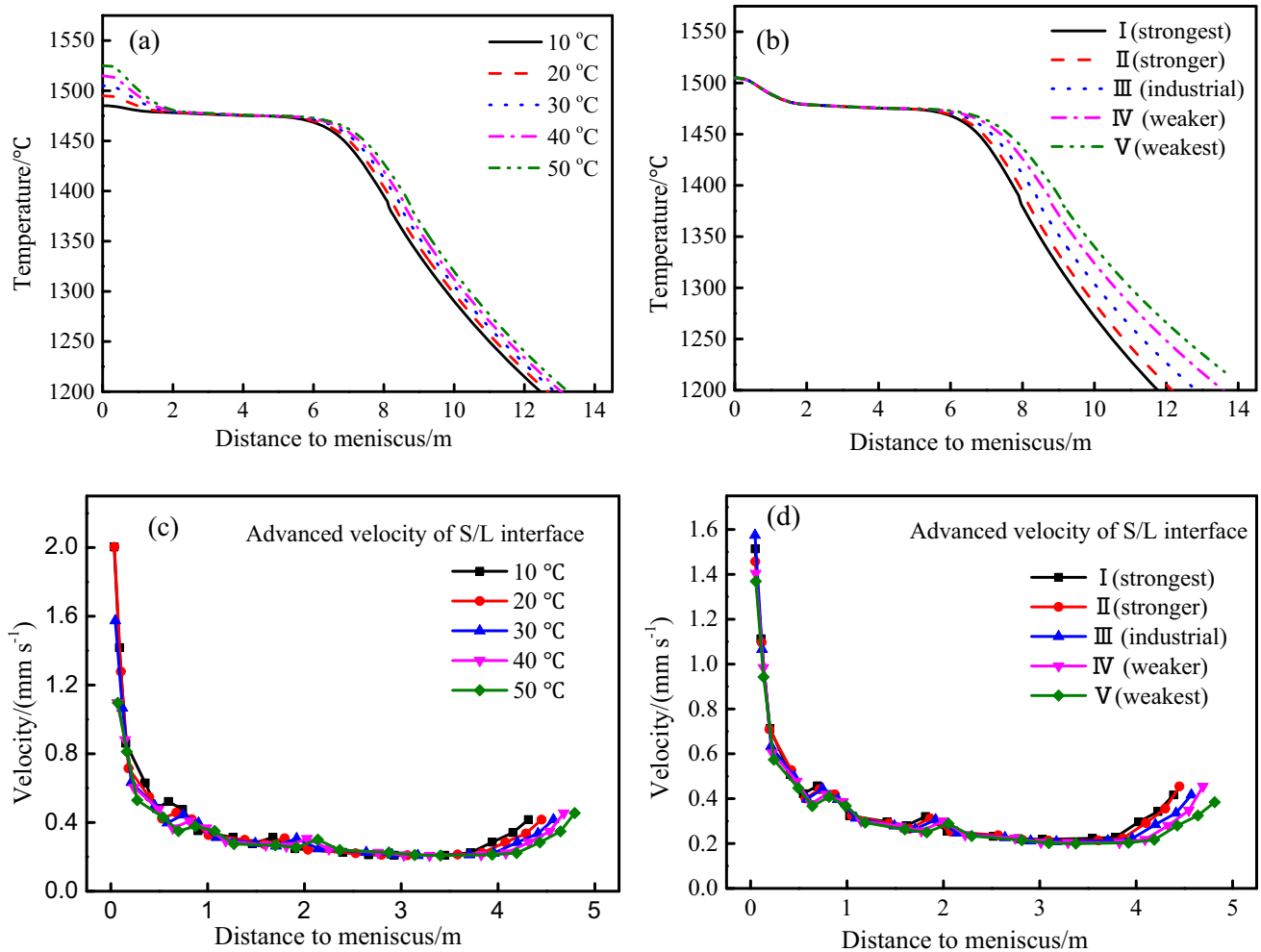


**Fig. 2** Cooling curves of high-temperature zone (a, b) and moving speed of heating unit (c, d) calculated by numerical simulation. a, c Cooling model III; b, d 30 °C superheat. S/L Solid/liquid

superheats are 10, 20, 30, 40 and 50 °C, while the cooling intensity is cooling modes I–V (as shown in Table 3). The length of each zone with different solidification conditions is shown in Fig. 4. The effects of superheat and cooling intensity on grain size in chill zone and center equiaxed zone are shown in Fig. 5.

The length of chill and equiaxed crystal zones decreases with the increasing superheat, while columnar zone increases. Nevertheless, the effects decrease as the superheat increases [25]. As superheat increases, the molten DSS melt or washed out the crystal nucleus on the surface of equiaxed grain in the chill zone. The chill zone thicknesses decreased from 19.58 to 13.47 mm with the superheat increasing (as shown in Fig. 4a). As shown in Fig. 3a, when the superheat is lower than or equal to 20 °C, columnar zone hardly exists. When the superheat is higher than or equal to 30 °C, the length of columnar zone increases slightly with superheat increasing (as shown in Figs. 3a and 4a). Lipton has reported that the condition for

the columnar-to-equiaxed transition (CET) is a reduction of superheat [25, 26]. The higher the superheat is, the longer it takes to reach the temperature which is necessary for unconstrained growth. The time for competitive growth of the columnar and equiaxed crystals is shorter. Consequently, columnar zone is longer.

CET position could reflect the equiaxed crystal ratio, which referred to the mean distance between chill surface and CET interface. CET shifts left with the superheat increasing (as shown in Fig. 4a). Thus, the percentage of equiaxed crystal zone decreases as the superheat increases. The percentage of equiaxed crystal zone is larger when the superheats are 10 and 20 °C, which is coincident with the previous researches that the equiaxed crystal zone increases at low superheat casting [5, 25]. Therefore, the superheat should be lower to increase the percentage of equiaxed crystal. As shown in Fig. 5a, the grain size in equiaxed crystal zone increases with the superheat decreasing. When the superheat is higher than or equal to 30 °C, the grain

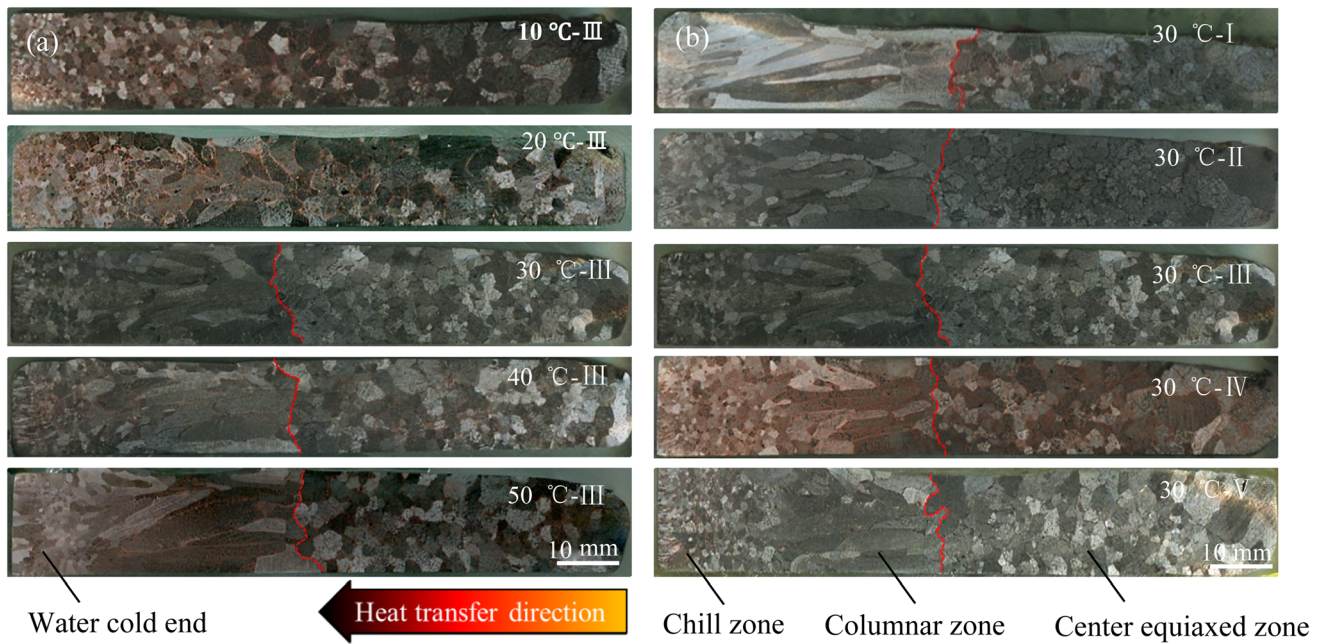


**Fig. 3** Macrostructure of DSS solidified with different superheat and cooling intensities. **a** Solidified with different superheats at cooling intensity III; **b** solidified at different cooling intensities with 30 °C superheat

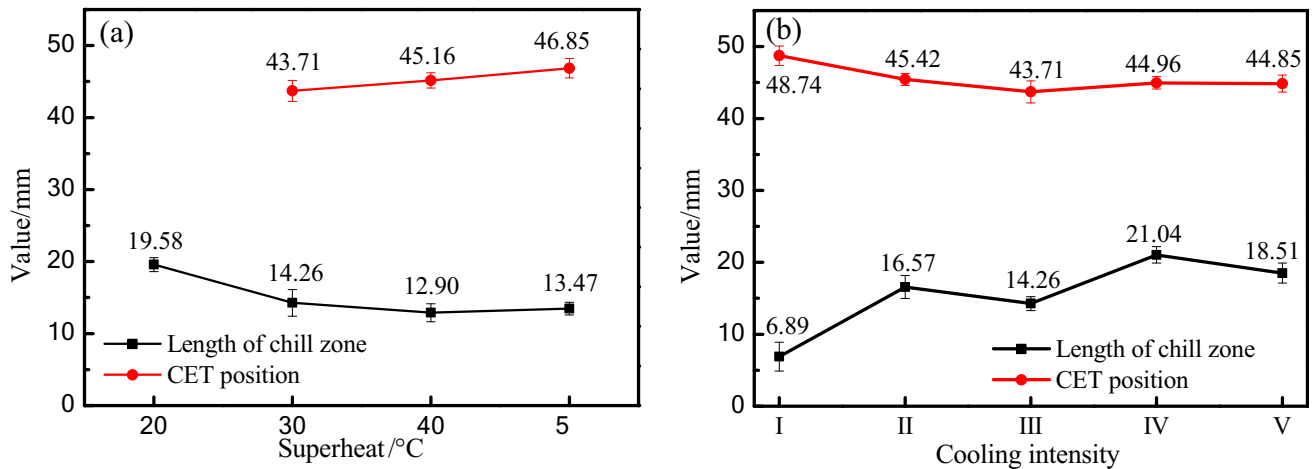


**Fig. 4** Effects of superheat **(a)** and cooling intensity **(b)** on CET position and columnar zone length of lean DSS TS samples

size hardly changes. Larger grain size should be undesired for the good performance. Fine equiaxed crystal is significant for the quality of continuous casting slabs, which could improve center segregation and mechanical properties. Taken together, 30 °C superheat should be better.

The length of chill zone zigzag increases with the cooling intensity weakening. In Fig. 4b, the length of chill zone increases from 6.89 to 18.5 mm with the cooling intensity weakening from cooling mode I to V. The grain size in chill zone firstly increases and then decreases slightly as the cooling intensity weakens (as shown in Fig. 5b). When the cooling mode is III, the grain size is largest. The columnar zone decreases with weakening

cooling intensity (shown in Fig. 4b). The position of CET gets closer to the cooling end with the cooling intensity weakening, which means that the percentage of equiaxed crystal increases (shown in Fig. 4b). When the cooling intensity is weaker than cooling mode III, however, CET position has little relation with cooling intensity. As shown in Fig. 5b, the grain size in equiaxed crystal zone increases slightly with cooling intensity weakening. The effects diminish as the cooling intensity weakens. The weakening of cooling intensity leads to the decrease in temperature gradient in the molten metal, which blocks the growth of columnar, and yet is beneficial for the equiaxed crystal. Figure 5 shows that mean grain size was mostly above

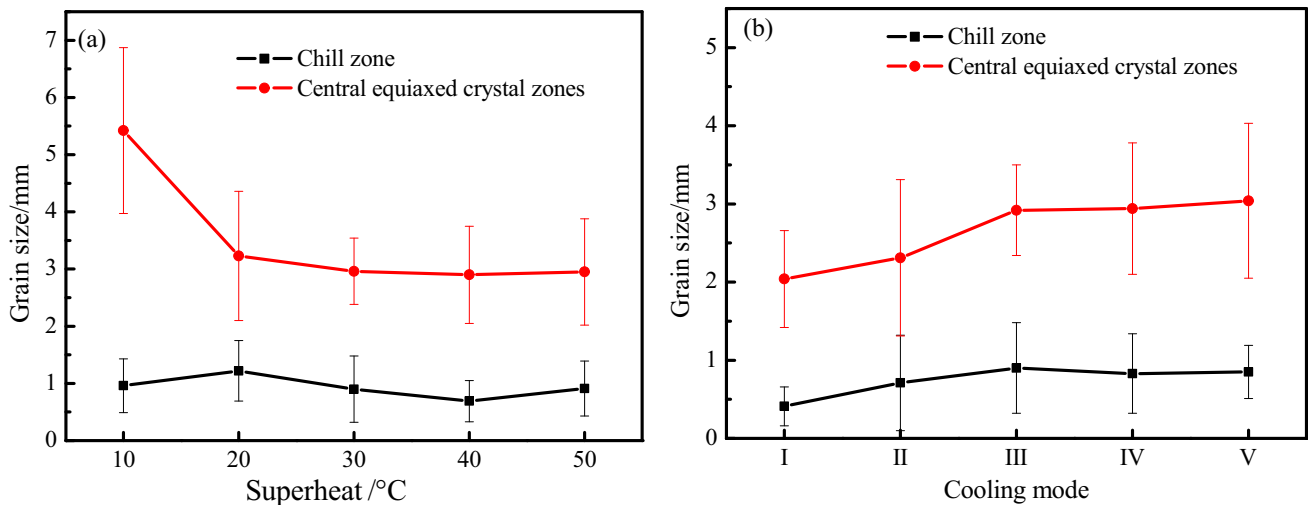


**Fig. 5** Effects of superheat (a) and cooling intensity (b) on grain size in chill zone and center equiaxed zone of lean DSS TS samples

2 mm [2], which implied that the nucleation rates of equiaxed grains in this DSS samples were less than  $10^9 \text{ m}^{-3}$ .

### 3.2 Macrosegregation

Macrosegregation refers to chemical variations over length scales approaching the dimensions of the casting, which leads to changeable microstructure and mechanical properties from centimeters or meters, and could hardly be eliminated by mechanical process or thermal treatment. Consequently, macrosegregation is undesirable for casting manufacturers. As shown in Table 1, Mn, Cr, Ni, Si, Cu and Mo are the main alloying elements for DSS, whose macrosegregation is studied by thermal simulation.

Macrosegregation index ( $K$ ) is used to characterize the segregation degree of TS samples, which is calculated based on the chemical composition detected by laser-induced breakdown spectroscopy through the following equation:

$$K = \frac{C_i}{C_0}, \quad (2)$$

where  $C_i$  is elements content at one detection point, wt.%; and  $C_0$  is average content, wt.%. Macrosegregation indexes with different superheats or cooling modes are shown in Fig. 6. When  $K$  is equal to 1, the elements are uniform distribution. If  $K$  is larger than 1, the elements are positive segregation. Instead, it is negative segregation. As shown in Fig. 6, the influences of cooling intensity on macrosegregation are greater than those of superheat. Slight gravity segregation of Cr appears. The value of  $K$  for Cr ranges from 0.96 to 1.04. Consequently, the distribution of Cr could be considered much more homogenous than that of other elements. The macrosegregation of Si is

serious, especially when the cooling intensity is mode V. As the cooling intensity is weakest, the solidification is slowest. There is enough time for the diffusion of Si. Consequently, obvious negative segregation is in the chill zone, while positive segregation is observed at the end of center equiaxed zone. For Mn, when the cooling intensity is strong, positive segregation appears in the chill zone due to the insufficient diffusion caused by quick solidification. When the cooling intensity weakens, positive segregation gets closer and closer to the end of TS samples.

In order to characterize the macrosegregation quantitatively, statistical segregation degree is calculated, which could reflect the uniform of elements distribution, and is closely related to the continuous caster process parameters. Figure 7 shows the statistical segregation degree of DSS solidified with different superheats and cooling modes. The greater the statistical segregation is, the more serious the macrosegregation is. As shown in Fig. 7a, the macrosegregation of Si, Mn and Cr is slightly dependent on superheat, while that of Cu, Mo and Ni changes greatly with superheat increasing. At the same solidification condition, the macrosegregation of Cu, Mo and Ni is much severer. For all the studied elements, when the superheat is 50 °C, the statistical macrosegregation degree is lowest. Figure 7b shows the influences of cooling intensity on the statistical macrosegregation degree. The variation of the statistical macrosegregation degree with cooling intensity changing is greater than that with the superheat, which is in coincidence with the results shown in Fig. 6. For Cr, Mo and Si, the macrosegregation is slightest when the cooling intensity is mode III. For Ni and Mn, the cooling mode II is most suitable. For Cu, cooling mode IV could ensure the most homogeneous distribution. Different elements require different solidification parameters to reduce its macrosegregation.

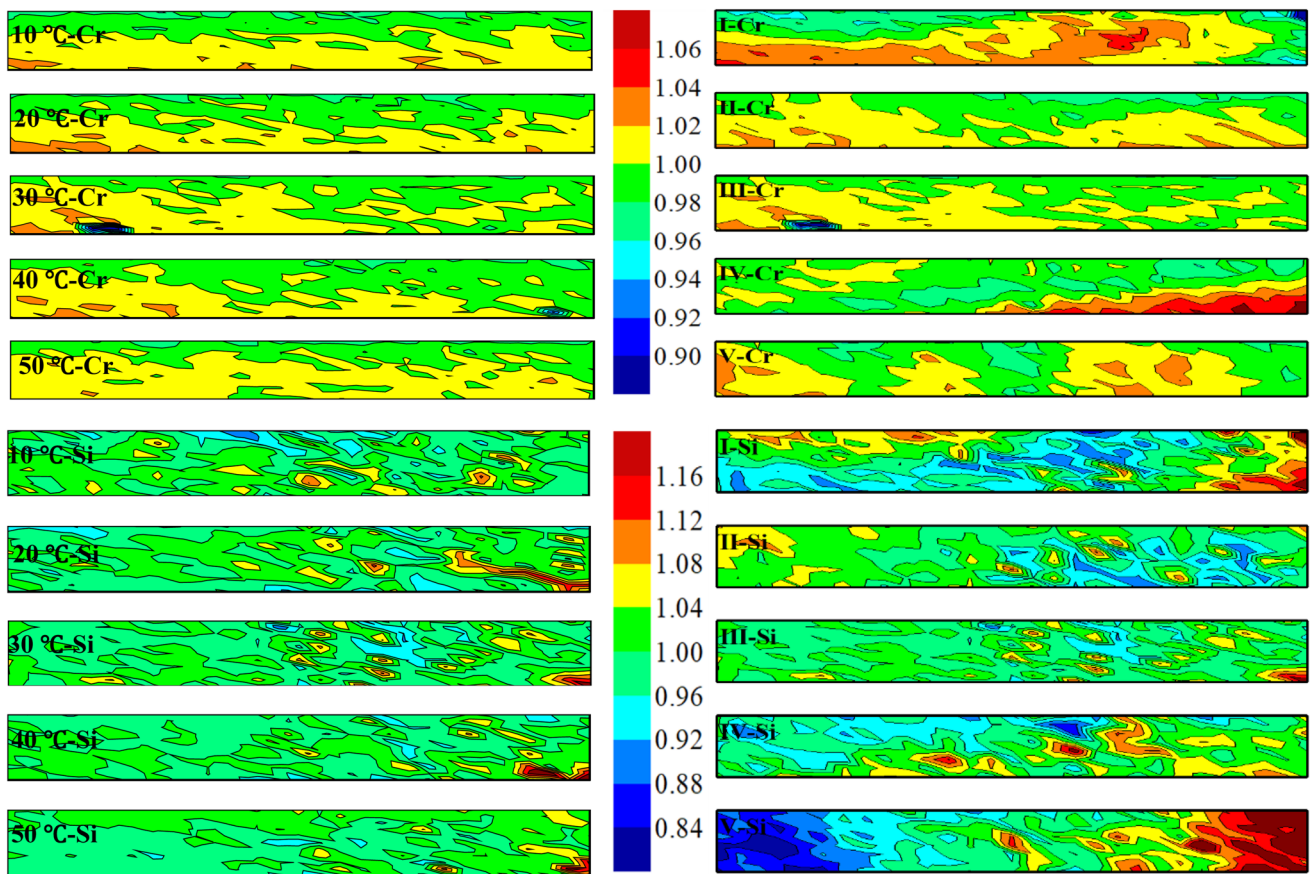


Fig. 6 Solutes distribution of Cr, Si and Mn in samples with different superheats and cooling modes

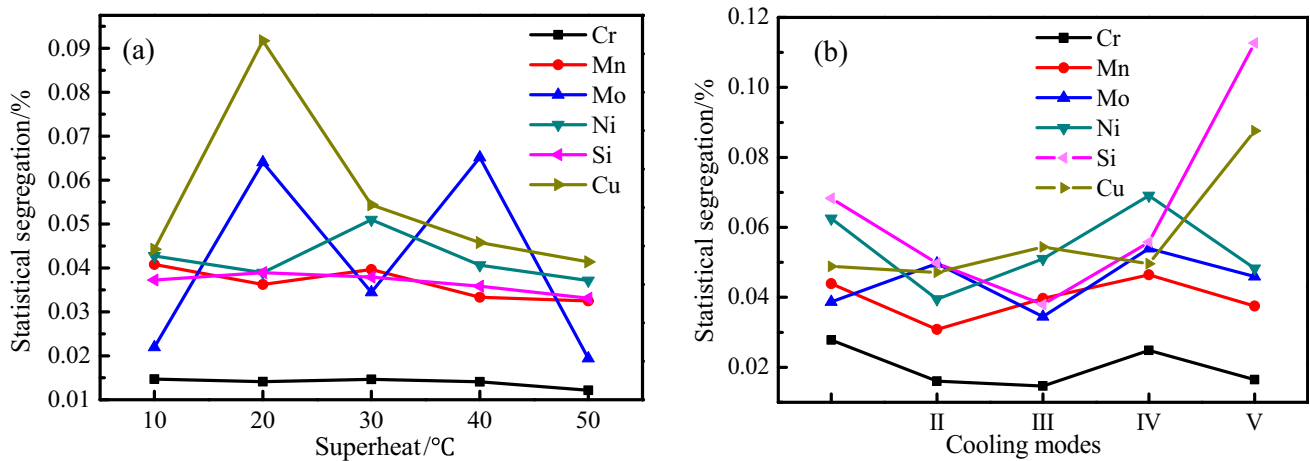


Fig. 7 Influences of superheat (a) and cooling modes (b) on statistical segregation of lean DSS TS samples

### 4 Conclusions

1. The macrostructure of DSS TS samples includes three zones: chill zone, columnar zone and center equiaxed zone. The length of each zone is affected by superheat and cooling intensities. The center equiaxed zone increases with the superheat decreasing. However, the

lower superheat leads to larger grain size, which is harmful for the performance of caster. The percentage of center equiaxed zone first increases and then decreases with the cooling intensity weakening, which obtains maximum value as the cooling intensity is mode III.

2. Statistical segregation degree is adopted to characterize the macrosegregation quantitatively. The macrosegregation of Si, Mn and Cr is slightly dependent on superheat, while that of Cu, Mo and Ni changes greatly with superheat increasing. When the superheat is 50 °C, the statistical segregation degree of all the studied elements is lowest. For Cr, Mo and Si, the macrosegregation is slightest when the cooling intensity is mode III. For Ni and Mn, the cooling mode II is most suitable. For Cu, cooling mode IV could ensure the most homogeneous distribution. As a whole, the influences of cooling intensity on macrosegregation are greater than those of superheat.

**Acknowledgements** This article is subsidized by National Key Research and Development Program of China (No. 2017YFB0701802) and NSFC (Nos. 51504148 and U1760204).

## References

- [1] H.M. Tawancy, N.M. Abbas, *J. Mater. Sci. Lett.* 7 (1988) 676–678.
- [2] J.O. Nilsson, A. Wilson, *Mater. Sci. Technol.* 9 (1993) 545–554.
- [3] Y.M. Jiang, T. Sun, J. Li, J. Xu, *J. Mater. Sci. Technol.* 30 (2014) 179–183.
- [4] Z.G. Song, H. Feng, S.M. Hu, *J. Iron Steel Res. Int.* 24 (2017) 121–130.
- [5] J.P. Liang, C.J. Song, L.X. Wang, Z.J. Li, Q.J. Zhai, *Mater. Technol.* 27 (2013) 333–336.
- [6] R.G. Santos, S.R. Andrade, J.L. Peralta, *Mater. Sci. Forum* 426–4 (2003) 1499–1504.
- [7] S.I. Chung, J.K. Yoon, *Ironmak. Steelmak.* 23 (1996) 425–432.
- [8] X.L. Liao, Q.J. Zhai, J. Luo, W.J. Chen, Y.Y. Gong, *Acta Mater.* 55 (2007) 3103–3109.
- [9] A.K. Hou, Q.L. Zhang, G.D. Xu, M.F. Jiang, *J. Iron Steel Res. Int.* 22 (2015) 98–103.
- [10] Q.T. Guo, M.H. Sha, J.X. Jia, X.L. Zhu, H. Zou, L.H. Cai, *J. Iron Steel Res. Int.* 22 (2015) 93–97.
- [11] Y. Xu, E.G. Wang, Z. Li, A.Y. Deng, *J. Iron Steel Res. Int.* 24 (2017) 483–489.
- [12] T. Sun, F. Yue, H.J. Wu, C. Guo, Y. Li, Z.C. Ma, *J. Iron Steel Res. Int.* 23 (2016) 329–337.
- [13] Y.Y. Gong, S.M. Cheng, Y.Y. Zhong, X. Wang, Y.H. Zhang, Q.J. Zhai, H.G. Zhong, Z.S. Xu, R. Yue, N. Pei, *J. Iron Steel Res. Int.* 25 (2018) 854–861.
- [14] S.M. Cheng, Y.Y. Zhong, Z.S. Xu, N. Pei, Q.J. Zhai, Y.Y. Gong, *Mater. Sci. Technol.* 34 (2018) 1212–1217.
- [15] D. Liang, J. Sun, T.Y. Liu, Q.J. Zhai, G. Wang, D.H. StJohn, H.B. Dong, H.G. Zhong, *Adv. Eng. Mater.* 17 (2015) 1465–1469.
- [16] Y.Y. Gong, J. Luo, J.X. Jing, Z.Q. Xia, Q.J. Zhai, *Mater. Sci. Eng. A* 497 (2008) 147–152.
- [17] J. Zhao, J.H. Yu, K. Han, H.G. Zhong, R.X. Li, Q.J. Zhai, *Acta Metall. Sin. (Engl. Lett.)* 31 (2018) 1334–1344.
- [18] H.G. Zhong, X.R. Chen, X.Y. Han, K. Han, Q.J. Zhai, *Metall. Mater. Trans. B* 47 (2016) 2963–2970.
- [19] L. Bai, B. Wang, H.G. Zhong, J. Ni, Q.J. Zhai, J.Y. Zhang, *Metals* 6 (2016) 53–64.
- [20] H.G. Zhong, J. Cheng, Z.S. Xu, Q.J. Zhai, *Shanghai Metals* 38 (2016) No. 2, 51–54.
- [21] B. Wang, H.G. Zhong, X.H. Li, X.B. Wang, T.M. Wu, Q.M. Liu, Q.J. Zhai, *Metals* 9 (2019) 249–261.
- [22] Q.J. Zhai, Y.Y. Gong, R.X. Li, *Journal Materials and Metallurgy* 14 (2015) No. 2, 81–82.
- [23] B.G. Thomas, I.V. Samarasekera, J.K. Brimacombe, *Metall. Trans. B* 15 (1984) 307–318.
- [24] Y.A. Meng, B.G. Thomas, *Metall. Mater. Trans. B* 34 (2003) 685–705.
- [25] B. Weisgerber, M. Hecht, K. Harste, *Steel Res.* 70 (1999) 403–411.
- [26] J. Lipton, W. Heinemann, W. Kurz, *Archiv für das Eisenhüttenwesen.* 55 (1984) 195–200.